

Amount of Mononuclear Phagocyte Infiltrate Does Not Predict Area of Experimental Choroidal Neovascularization (CNV)

Adrian Will-Orrego,* Yubin Qiu,* Elizabeth S. Fassbender, Siyuan Shen, Jorge Aranda, Namrata Kotagiri, Michael Maker, Sha-Mei Liao, Bruce D. Jaffee, and Stephen H. Poor

Abstract

Purpose: Mononuclear phagocytes (MNPs) are present in neovascular age-related macular degeneration (nv AMD) which is also called choroidal neovascularization (CNV). The number and phenotype of the MNPs depend upon the local environment in the CNV and effect of nv AMD therapy. We investigated ocular cell infiltration and conditions that modulate angiogenesis in a laser-induced mouse CNV model.

Methods: We developed assays to quantify MNPs in our established mouse CNV model. One MNP assay quantified the number of subretinal cells peripheral to the CNV lesions. A second assay semiquantitatively assesses the number of MNPs localized to the CNV lesion. We used these assays to measure the effect of toll-like receptor-2 (TLR-2) activation, anti-vascular endothelial growth factor (VEGF) therapy, and chemokine (C-C motif) ligand 2 (Ccl2) genetic deletion on MNP infiltration after laser injury.

Results: Laser injury induced blood vessel growth and infiltration of MNPs. Systemic administration of a TLR-2 activating peptide increased laser-induced CNV area, MNP cell numbers, and MNP density over the CNV lesions. Systemic administration of a VEGF antibody reduced CNV area, while Ccl2 genetic deletion increased CNV area. Despite the change in amount of angiogenesis, MNP infiltration was, surprisingly, unchanged in these 2 conditions.

Conclusions: MNP quantification provides biological insights for candidate AMD therapies. The number of infiltrating MNP cells does not correlate with the amount of laser-induced CNV area.

Keywords: microglia, MNPs, CNV, anti-VEGF, TLR-2, angiogenesis

Introduction

AGE-RELATED MACULAR DEGENERATION (AMD) is a common cause of vision loss and morbidity in the elderly.¹ Chronic inflammation, cellular infiltrates, and immune responses to extracellular deposits are features of AMD pathology.^{2,3} Advanced AMD can result in debilitating vision loss⁴ and is associated with either pathological blood vessel growth from the choroid [neovascular AMD (nv AMD)] and/or widespread retinal pigment epithelium (RPE) and photoreceptor death (geographic atrophy). A key feature of AMD is an infiltrate of mononuclear phagocytes (MNPs). MNPs are microglia, resident immune cells, or tissue infiltrating macrophages. MNPs are present around drusen, areas of RPE

atrophy, and in choroidal neovascularization (CNV).⁵⁻⁸ Current therapy for nv AMD is regular intravitreal injections of vascular endothelial growth factor (VEGF) blocking biologic reagents, while there is no treatment for geographic atrophy.^{9,10} Understanding how MNP cellular infiltrates affect blood vessel growth and ocular cell function and modification of these effects by candidate drug targets will be important for the development of the next generation of AMD therapeutics.

In healthy eyes, microglia are present in the inner retina. Microglia maintain homeostasis by surveying the retina for any debris, apoptotic cells, or damaged DNA. In the healthy state, microglia are benign, phagocytosing but not presenting antigen nor inducing an inflammatory response.^{11,12} Danger signals activate microglia, inducing a graded change

Department of Ophthalmology, Novartis Institutes for Biomedical Research, Cambridge, Massachusetts.

*Joint first authors.

© Adrian Will-Orrego et al., 2018; Published by Mary Ann Liebert, Inc. This Open Access article is distributed under the terms of the Creative Commons Attribution Noncommercial License (<http://creativecommons.org/licenses/by-nc/4.0/>) which permits any non-commercial use, distribution, and reproduction in any medium, provided the original author(s) and the source are cited.

in morphology, gene expression, and migration toward the danger signal. In AMD, microglia migrate toward the outer retina. With chronic activation, microglia release excessive inflammatory and angiogenic factors that cause both neuronal and RPE degeneration.^{13,14} Factors contributing to chronic retinal microglia activation include aging, pro-inflammatory cytokines, complement activation products, lipofuscin, oxidized lipid deposits, and photoreceptor debris.^{6,15–17} Toll-like receptors (TLRs) are transmembrane RPE and MNP receptors recognizing foreign or abnormal materials and alert immune cells to potential danger.^{18–20} Endogenous oxidized lipids and phospholipids, present in ocular lipid deposits, induce inflammation and angiogenesis through TLR-2 activation.^{21–25} Experimental and newly formed human CNV is associated with MNP infiltrates,^{5,26} and in the latter, the CNV advances through layers of age-related lipid deposits below the RPE^{27,28} linking oxidized lipids, TLR-2, and AMD progression. Infiltrating cells may be of therapeutic or injurious effect depending upon the stage of the disease and the phenotype of the cells.²⁹

Chemokine (C-C motif) ligand 2 (Ccl2) is a chemoattractant protein recruiting chemokine (C-C motif) receptor 2 (Ccr2) expressing immune cells, including MNPs to sites of inflammation. Ccl2 genetic deletion reduces macrophage recruitment in inflammatory models (eg, inflammation in peritoneum, lung, and brain^{30–32}). Ccl2 genetic deletion has variable ophthalmic effects, including protection and accelerated degeneration of the retina, as well as reduction in angiogenesis.^{33–36} Increased intraocular Ccl2 has been reported in geographic atrophy and nv AMD patients,³⁷ and increased subretinal infiltration of Ccr2⁺ cells has been observed in patients.³⁵

Laser pulse rupture of Bruch's membrane rodents is followed by the production of angiogenic and inflammatory cytokines, an influx of inflammatory cells, and growth of choroidal blood vessels into the subretinal space.³⁸ To investigate the relationship of MNP cell infiltration and vessel growth, we evaluated the effects of TLR-2 activation, VEGF inhibition, or genetic deletion of Ccl2 in our established laser-induced CNV model and investigated MNP infiltration using 2 novel assays.

Methods

Type, origin, and selection of mice

Animal research presented in this article was approved by the Novartis Institutes for Biomedical Research IACUC and adhered to the ARVO Statement for the Use of Animals in Ophthalmic and Vision Research.

Mice used in a single experiment arrived at our research facility in a single shipment and were age and sex matched.

Female C57BL/6NTac mice were purchased from Taconic (Tarrytown, NY) and were typically 8–10 weeks old and were used in all studies unless otherwise specified. TLR-2 KO (B6.129S1-Tlr2tm1Degen), Ccl2 KO (B6.129S4-Ccl2tm1Rol), and C57BL6/J were acquired from The Jackson Laboratory (Bar Harbor, ME). Heterozygous TLR-2 and heterozygous Ccl2 mice were generated in the Novartis breeding facility by crossing respective KO mice with Jax C57BL6/J mice. All mice were bred to be wild type for crumbs homolog 1 (Crb1). The TLR-2 KO, Ccl2 KO, and their wild-type littermate sex-matched control mice used in

our studies were produced from mating of TLR-2 and Ccl2 heterozygous mice, respectively. All mice used in our studies were genotyped using the protocol from The Jackson Laboratories (Stock number 005846 and 004434).

Laser photocoagulation

Laser pulses rupture Bruch's membrane due to the absorption of laser energy by the RPE resulting in focal cell death and generation of cellular debris. Microglia and/or macrophages are reported to infiltrate into sites of laser injury contributing to the development of CNV.^{26,39,40}

CNV was induced by laser injury as previously described.³⁸ The CNV area was measured 7 days after the procedure. Tissue processing, application of exclusion criteria, and CNV area quantification were performed as previously described.³⁸

Reagents assessed for modulation of laser-induced CNV

PAM3CSK4 is a synthetic diacylated lipopeptide activating TLR-2 with cooperation from TLR-1. PAM3CSK4 (InvivoGen, San Diego, CA) was dissolved in sterile endotoxin free water to a final concentration of 0.5 mg/mL. Mice were injected intraperitoneally (i.p.) with 50 µg of PAM3CSK4 (henceforth referred to as PAM) solution or control [sterile endotoxin free water or sterile phosphate buffered saline (PBS)]. In time course studies of laser-induced CNV area, a single dose of PAM was injected at either day 0, 1, 2, 3, or 4 relative to laser application. For subsequent studies, single i.p. injections of PAM or vehicle control (either sterile water or PBS) were administered 2 days after laser application.

4G3 is a human Fab converted to a full-length IgG antibody with a mouse IgG1 Fc tail.³⁸ 4G3 binds to mouse VEGF₁₆₄ with a dissociation constant of 10 pM and neutralizes mouse VEGF binding to human VEGFR2 with an EC₅₀ of 0.15 nM in a binding assay (ELISA; MSD, Rockville, MD).³⁸ For efficacy studies in the mouse laser CNV assay, 4G3 dissolved in PBS was dosed i.p. at doses of 0.1, 0.3, 1.0, 3.0, or 10 mg/kg at day 0, 2, and 4 after laser. Either rat IgG_{2a} isotype (MAB006; R&D systems, McKinley Place, MN) dissolved in PBS or PBS was dosed i.p. as negative controls for laser CNV studies.

Cellular infiltration assay

Cellular infiltration into the posterior eye cup (PEC, composed of the RPE, choroidal, and scleral tissues) was assessed after laser application. Eyes were fixed with 4% paraformaldehyde (Fisher Scientific, Hampton, NH) for 90 min. After fixation, the retina was dissected from the PEC. Next, the tissues were processed for flat mounts. The tissues were blocked in PBS with 1% bovine serum albumin (BSA) (EMD Millipore, Billerica, MA) for 1–2 h. PECs were incubated overnight with rabbit anti-mouse ionized calcium binding adaptor molecule-1 (Iba1, 019-19741; Wako Chemicals, Cambridge, MA) 1:1,000 to label microglia and/or macrophages (MNP cells found in ocular tissues) and biotin-Ly-6G/C, also known as Gr1 (108403; BioLegend, San Diego, CA), 1:1,000 in staining buffer to label neutrophils. Tissues were washed with washing buffer (1% BSA in PBS) 3 times each for 20 min. The PEC was incubated for 2 h with anti-rabbit Alexa Fluor 488 (A-21206; Thermo) 1:1,000 and Streptavidin Alexa Fluor 594 (S32356; Thermo) in 1% BSA

and 0.5% Triton X-100, in PBS. Tissues were then washed with washing buffer 3 times each for 15 min. Tissues were flat mounted with VECTASHIELD with DAPI (Vector Laboratories, Burlingame, CA).

Imaging of cellular infiltration

Flat mounted PECs were imaged with a Zeiss Axio Imager M1 fluorescent camera at different magnifications. To visualize the infiltrating Iba1⁺ cells in the PEC and CNV, images at 5× magnification of the PEC were captured centered on the optic nerve covering ~70% of the tissue. Images of Gr-1⁺ neutrophils in CNV lesions were captured at 20× magnification.

Analysis of intensity of Iba1⁺ label and neutrophil count on CNV lesions

Iba1⁺ label intensity on the CNV lesion was assessed with a semiautomated MATLAB (MathWorks, Natick, MA) code; an overview of protocol for this analysis is presented in Supplementary Fig. S1; Supplementary Data are available online at www.liebertpub.com/jop A threshold value for each experiment was determined by measuring the mean threshold of Iba1⁺ label in 10 representative 5×PEC images. The mean threshold value was applied to all images in the experiment for analysis of integrated density. A radius of the region of interest (ROI) was determined by selecting a size that overlapped 10 representative CNV lesions. For all experiments presented, the selected ROI radius was 65 pixels (266.5 microns). The operator placed 3 ROIs per image, 1 on each individual CNV. The MATLAB software calculates the number of pixels above the threshold value in the ROI and the mean gray value of those pixels. The integrated density of Iba1⁺ label per CNV is the product of the number of pixels above threshold in the ROI and the mean gray value of pixels in the ROI (Methods adapted from <http://rsb.info.nih.gov/ij/docs/menus/analyze.html>).

CNV Lesions were excluded from analysis 1) if the CNV was obscured by a hemorrhage, 2) if there was obvious anatomical damage, or 3) if the CNV lesion was not fully captured in the image. The MATLAB code can be found at <https://github.com/Novartis>

Gr1⁺ cells in the CNV lesion were counted manually on masked randomized 20× images. CNV lesions were excluded from the quantification if a large hemorrhage or anatomical damage from tissue processing obscured the CNV.

Peripheral cell count

Iba1⁺ cells in the PEC are sparsely distributed around the PEC, except at the CNV. Single cells are easier to quantify than confluent overlapping microglia. Therefore we developed a second semiautomated MATLAB code to quantify single Iba1⁺ cells. Clustered microglia external to the CNV lesion were rare and excluded from the cell count. The operator was then presented with masked, randomized 5× magnification images and allowed to remove nonspecific fluorescence (false positive) and/or add missed cells (false negative) to the analysis. Clustered microglia cells and CNV lesions were excluded from the quantification analysis. Eyes were excluded from the analysis if large hemorrhage or

anatomical damage from tissue processing covered more than 10% of the tissue. The MATLAB code can be found at <https://github.com/Novartis>

Statistical analysis

Analyses and exclusions were performed on masked and randomized images. CNV area between groups was analyzed with either an one-way analysis of variance (ANOVA) using Prism version 6 software (GraphPad, Inc., San Diego, CA) for Windows (Microsoft, Redmond, WA) with Dunnett's *post hoc* analysis test or with an unpaired *t*-test.

Cellular infiltration and integrated density assays were analyzed with one-way ANOVAs using Prism with a Bonferroni's post-test or an unpaired *t*-test.

Anti-VEGF antibody 4G3 is a positive control in our laboratory for the mouse CNV assay. The ED₅₀ (dose achieving 50% efficacy) curve of anti-VEGF 4G3 was generated in Excel/XLfit (version 5.2.0.0:ID Business Solutions Ltd., Guildford, UK) with results from the 27 experiments, using a dose-response 1-site fit, with sigmoidal dose-response model, without parameter constraints.

Results

Laser injury induces Iba1⁺ cellular infiltration into the subretinal space

Mice eyes were lasered and collected for quantification of Iba1⁺ cells in the subretinal space at various time points after laser injury. Contemporaneously anesthetized mice without laser application were used as controls.

Control mice had an even distribution of Iba1⁺ cells around the optic nerve head. The numbers of Iba1⁺ cells decrease toward the edge of the flat mount, and on rare occasion Iba1⁺ cells cluster in 1 quadrant of the flat mount. Infiltrating Iba1⁺ cells are present 1 day after laser injury and still present 28 days later. The CNV lesions were enveloped with Iba1⁺ cells (Fig. 1A). Iba1⁺ cells peripheral to the CNV lesion are discrete and have a typical morphology and a robust signal allowing for semiautomated quantification (Fig. 1B, C).

After laser, Iba1⁺ cells in some eyes are evenly distributed around the 3 CNV lesions, while in other eyes, the cells migrated predominantly to 1 CNV lesion. The mechanism behind asymmetric infiltration of CNV lesions is unclear. The number of Iba1⁺ cells peripheral to the CNV increased by an average of 33% and 48% at day 3 and 7, respectively, ($P < 0.01$ and < 0.0001) after laser compared to nonlasered naive mice (Fig. 1D). This underestimates the overall number of infiltrating MNPs as the CNV lesions are not part of this analysis.

TLR-2 activation enlarges CNV area

TLRs are expressed on sentinel cells, including macrophages and microglia, and are involved in the activation of the innate immune response.⁴¹ Systemic administration of PAM, a TLR-2 activator, consistently increased CNV size compared to CNV in mice injected with PBS (Fig. 2). Single doses of PAM were injected i.p. into cohorts of mice either on the day of laser application or 1, 2, 3, or 4 days after laser and CNV area compared to mice injected with PBS. PAM injection increased CNV area with the largest effect

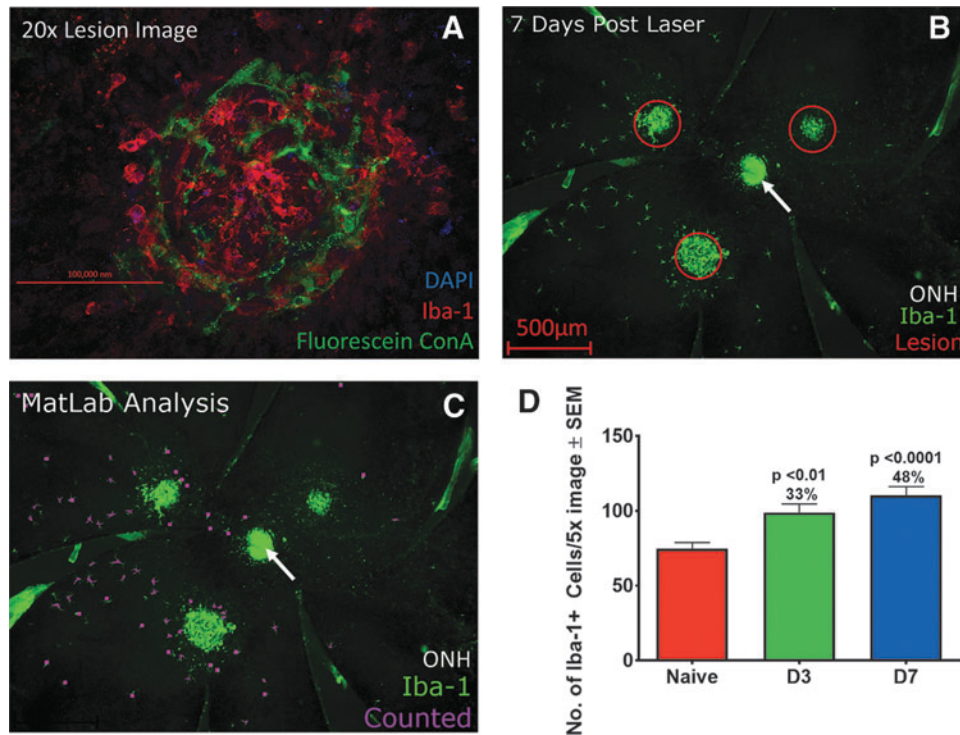


FIG. 1. Laser induced injury to mouse eyes induces Iba-1⁺ cellular infiltration into the subretinal space. **(A)** 20× confocal image of overlapping confluent Iba-1⁺ cells (green) on top of a CNV lesion labeled with Fluorescein Concanavalin A in a mouse PEC collected 7 days after laser application. **(B)** 5× image of a mouse PEC 7 days after laser injury applied in 3 regions. **(C)** Same image as **(B)**, with individual Iba-1⁺ cells peripheral to the CNV highlighted in purple by MATLAB analysis software. **(D)** Bar graph of number of Iba-1⁺ cells in the subretinal space of RPE-choroid flat mounts, peripheral to the CNV at day 3 (D3) and day 7 (D7) compared with naive nonlasered PEC ± SEM. Day 7 lasered mice exhibited the highest cellular infiltrate compared to the nonlasered mice. Iba1⁺ cell counts were analyzed in nonlasered mice collected either 3 or 7 days after anesthesia. As microglia counts were similar in nonlasered mice at both time points, these nonlasered mice were combined into 1 group for comparison to the lasered mice. Data presented are the number of peripheral microglia in 1 PEC sample ± SEM and are combined from 8 individual studies, $n=66-97$ data points for each condition. Scale bar figure **(A)** 200 μm, **(B)** 500 μm. ONH, optic nerve head (arrow). CNV, choroidal neovascularization; PEC, posterior eye cup; RPE, retinal pigment epithelium.

observed in mice injected on day 2 (Fig. 2A, B). Mice injected with PAM at day 2 had a mean CNV area $63\% \pm 18\%$ larger than in mice injected with PBS, replicated in 4 independent studies ($P \leq 0.003$ in each study).

TLR-2 activation increases Iba1⁺ and GR1⁺ cell infiltration into the subretinal space

We investigated the effect of TLR-2 activation by systemic PAM injection 2 days after laser, on Iba1⁺ infiltration. This time point was chosen due to the maximal effect on angiogenesis (Fig. 2).

Utilizing the MATLAB program described above, the numbers of individual Iba1⁺ cells peripheral to the CNV lesion were found to be increased at day 3 and 7 post laser in mice administered PAM compared to mice administered vehicle (Fig. 3A, B). This effect was observed in a pilot study and confirmed in a second study. In the second study ($n=5$ mice, 10 eyes per group), Iba1⁺ cell numbers were increased at day 3 by 89% ($P < 0.0001$) and at day 7 by 53% ($P < 0.05$) compared to mice injected with vehicle (Fig. 3C, D).

To analyze the Iba1⁺ cells infiltrating the CNV lesion area, we developed a second MATLAB program to measure the intensity of Iba1⁺ label in a defined ROI, centered on the CNV lesion (methodology in Supplementary Fig. S1). This

analysis is an indirect measurement of MNP cell number infiltrating the CNV. We found Iba1⁺ integrated density in the ROI increased in mice administered PAM3 compared to mice administered vehicle, at both days 3 and 7 after laser. This effect was observed in a pilot study and confirmed in a second study. In the second study, Iba1⁺ integrated density in PAM injected mice compared to vehicle injected mice increased at day 3 by 47% ($P < 0.01$) and day 7 by 124% ($P < 0.01$, $n=10$ eyes, 5 mice, 24–30 data points/group, Fig. 3E, F).

GR1⁺ cells are discrete, have a robust signal, and are typically localized to the CNV lesion (3 G & H). We manually quantified the number of GR1⁺ neutrophils in CNV lesions after laser in mice injected with PAM or with vehicle (Fig. 3I). We found that PAM administration increased the number of neutrophils at day 3. Mean number of neutrophils at day 3 increased from 1.3 to 13.7 neutrophils per CNV lesion ($P < 0.0001$, $n=4-5$ mice, and 23–30 CNV analyzed per condition). At day 7, neutrophils were minimally present in either group.

PAM administration has no effect on CNV area in TLR-2 KO mice

PAM activates the pro-inflammatory transcription factor NF-κB (nuclear factor kappa-light-chain-enhancer of activated

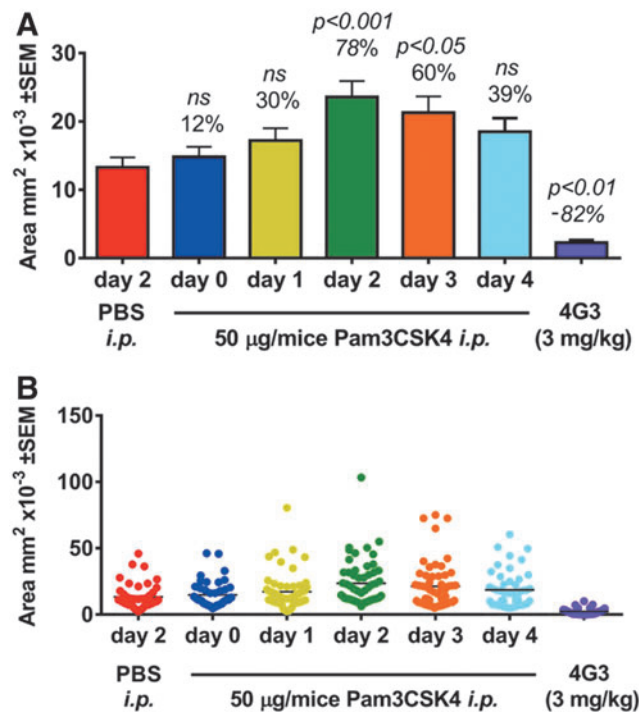


FIG. 2. Systemic administration of a TLR-2 activator increases laser-induced CNV area. **(A)** Bar graph and **(B)** *Dot plot* of area of CNV \pm SEM from an experiment evaluating the area of CNV. Mouse eyes were lasered on day 0, PAM injections were administered to cohorts of mice on different days in relation to the laser application, and CNV area was measured at day 7. Number above the bar is the percentage change relative to the average area of CNV in PBS treated mice. PAM injections increased CNV area with the largest effect observed in mice injected 2 days after laser. CNV area was reduced in mice administered doses of a VEGF Ab, 4G3, at 3 mg/kg i.p. on day 0, 2, and 4. $n = 39$ – 58 data points for each group. Statistical analysis performed with an ANOVA with a Dunnett's *post hoc* test with the PBS treated group as the comparator. $P > 0.05$. ANOVA, analysis of variance; PBS, phosphate buffered saline; ns, not significant; TLR-2, toll-like receptor-2; VEGF, vascular endothelial growth factor.

B cells) by binding to TLR-1 and TLR-2 (www.invivogen.com/pam3csk4). We investigated the effect of TLR-2 engagement and NK- κ B activity on CNV growth using TLR-2 KO mice and wild-type littermate sex-matched controls with and without PAM treatment. CNV area was larger in wild-type mice injected with PAM compared to water controls. In contrast, CNV area was similar in size in TLR-2 KO mice injected with PAM or water, $n = 2$ studies (Fig. 4A–D). Therefore, angiogenesis is enhanced by the activation of NF- κ B induced by the engagement of TLR-2 by PAM.

VEGF antibody dose dependently inhibits CNV area

The laser-induced CNV model is VEGF dependent. The CNV lesion area is reduced by blocking VEGF or VEGF receptors and increased by intraocular injection of VEGF.³⁸ A research grade VEGF blocking antibody, 4G3, dose dependently inhibits CNV growth and is a positive control reagent for our laser model. Representative CNV images of mice administered 4G3 or control and a dose–response

study of the effects of 4G3 reducing laser-induced CNV area are presented in Fig. 5A–C. Analyzing 4G3 data from 27 mouse laser CNV studies, the ED₅₀ (efficacious dose with 50% efficacy) of systemically dosed 4G3 is 0.49 mg/kg (Fig. 5D).

Iba1⁺ infiltration following laser is not reduced by VEGF Ab therapy

Microglia cells secrete VEGF and modulate vessel growth and wound healing.^{42,43} Antibodies blocking VEGFR1 but not VEGFR2 reduce microglia infiltration in experimental CNV.⁴⁰ *Iba1*⁺ cell infiltration was analyzed in mice administered VEGF blocking antibody (4G3) with a dosing regimen that inhibits CNV area by $\sim 70\%$ (3 mg/kg $3 \times$ per week).

The number of peripheral subretinal *Iba1*⁺ cells and the integrated density of *Iba1*⁺ label on CNV lesions in mice administered 4G3 or control were similar ($n = 4$ studies, $P > 0.05$ for each study, representative PEC images, and data presented in Fig. 6A–F).

Ccl2 KO mice exhibit larger CNV area compared to wild-type littermate controls

Macrophages are involved in wound healing, angiogenesis, and inflammatory responses after laser injury. We therefore assessed the role of *Ccl2* in the CNV model. Unexpectedly, CNV area significantly increased in *Ccl2* KO mice in 3 out of 4 studies compared to wild-type littermate sex-matched controls (Fig. 7A–D).

Ccl2 KO has minimal effect on numbers of infiltrating inflammatory cells

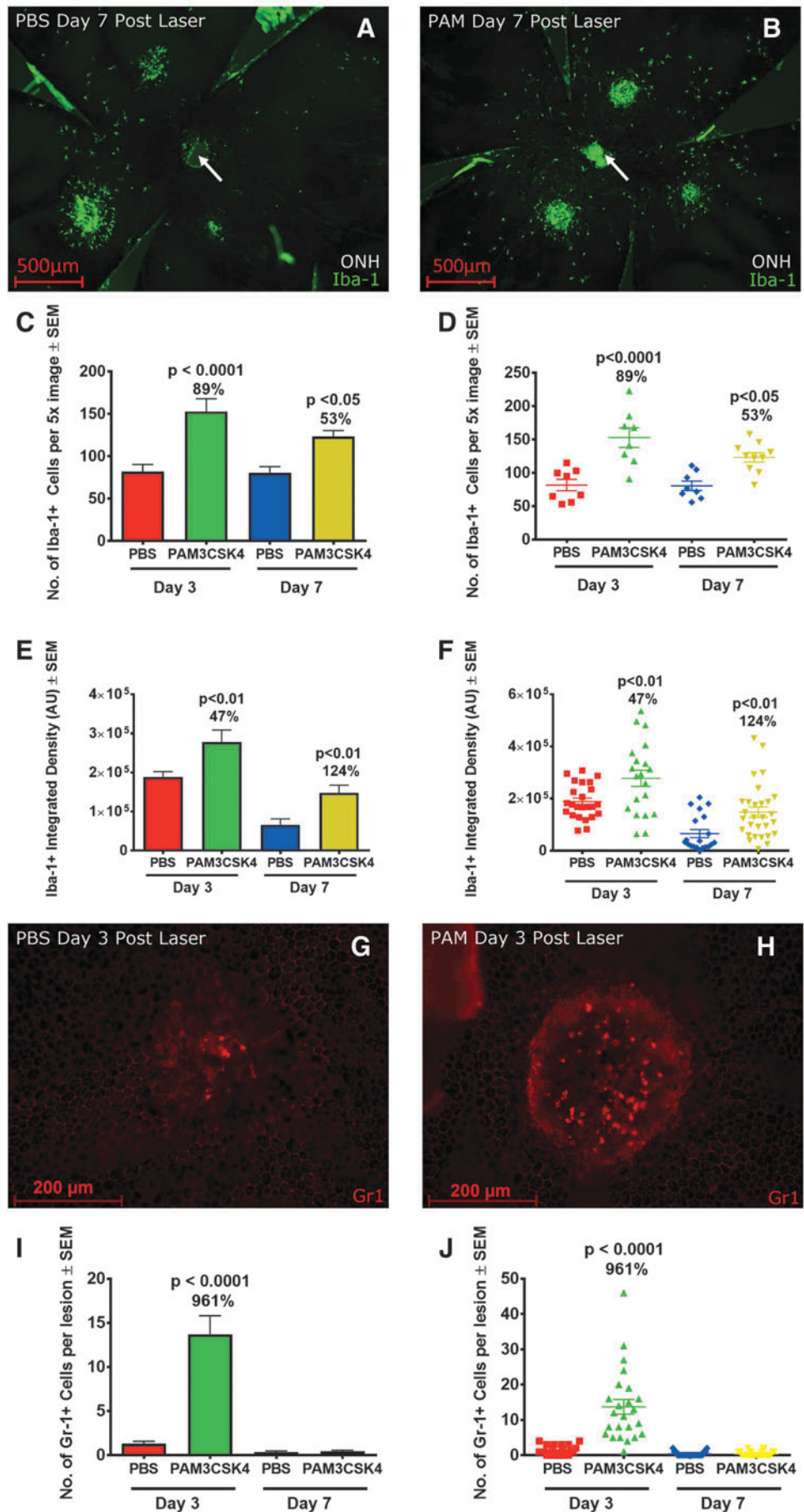
Iba1⁺ cell infiltration after laser was analyzed in *Ccl2* KO mice and wild-type littermate controls. The numbers of infiltrating *Iba1*⁺ cells post laser application between the KO and littermate control mice were similar (4 of 5 studies $P > 0.05$), an increase was observed in *Ccl2* KO in 1 of 5 studies ($P = 0.0464$, Supplementary Fig. S2). Integrated density of *Iba1*⁺ label on CNV was similar between KO and WT mice in 2 studies and modestly reduced in a third study (Supplementary Fig. S3). These results suggest that *Ccl2* genetic deletion has either no effect or at most a small effect on MNP infiltration after laser injury.

Discussion

Iba1⁺ cells rapidly infiltrate the subretinal space after laser injury and migrate to the laser-induced CNV lesion, which is enveloped in *Iba1*⁺ cells. These cells are a combination of local and infiltrating MNPs from the systemic circulation.^{44,45} We developed 2 methodologies quantifying the number of infiltrating cells in experimental CNV. Cell counting is a straightforward approach to analyze the subretinal environment peripheral to the CNV lesions. Fluorescent intensity measurements of the *Iba1*⁺ label indirectly quantify MNP directly at the CNV. These methods are complementary to other published techniques that analyze MNP morphology (activated vs. quiescent morphology on flat mounts) or FACS analysis of macrophages in ocular tissues with immunophenotyping.^{46,47}

Oxidized lipids, as found in AMD or retinitis pigmentosa, can activate TLR inducing inflammation and cellular infiltration.^{8,48,49} In addition, TLR activation contributes to RPE

FIG. 3. Systemic administration of PAM increased the number of Iba-1⁺ cells in the subretinal space, over the CNV lesion, and increased neutrophil infiltration into the CNV lesion after laser injury. Representative 5× image of a mouse PEC 7 days after laser injury in mice injected with (A) Vehicle or (B) PAM. (C) Bar graph and (D) Dot plot from a study demonstrating the number of Iba-1⁺ cells in mice injected with PAM ($n=8-10$ eyes of 4-5 mice per condition, $P<0.05$). (E) Bar graph and (F) Dot plot of mean intensity of Iba-1⁺ label on CNV lesions ($n=8-10$ eyes, 20-29 CNV analyzed per condition, $P<0.01$). 20× images of CNV labeled with Gr1 from mice treated with PBS (G) or PAM (H) Collected 3 days after laser. (I) Bar graph and (J) Dot plot of number of Gr1⁺ neutrophils per CNV lesion ($P<0.001$ at day 3, >0.05 at day 7). Scale bar (A) and (B) 500 μm and (G) and (H) 200 μm. Statistics performed with an unpaired *t*-test. ONH, optic nerve head (arrow).



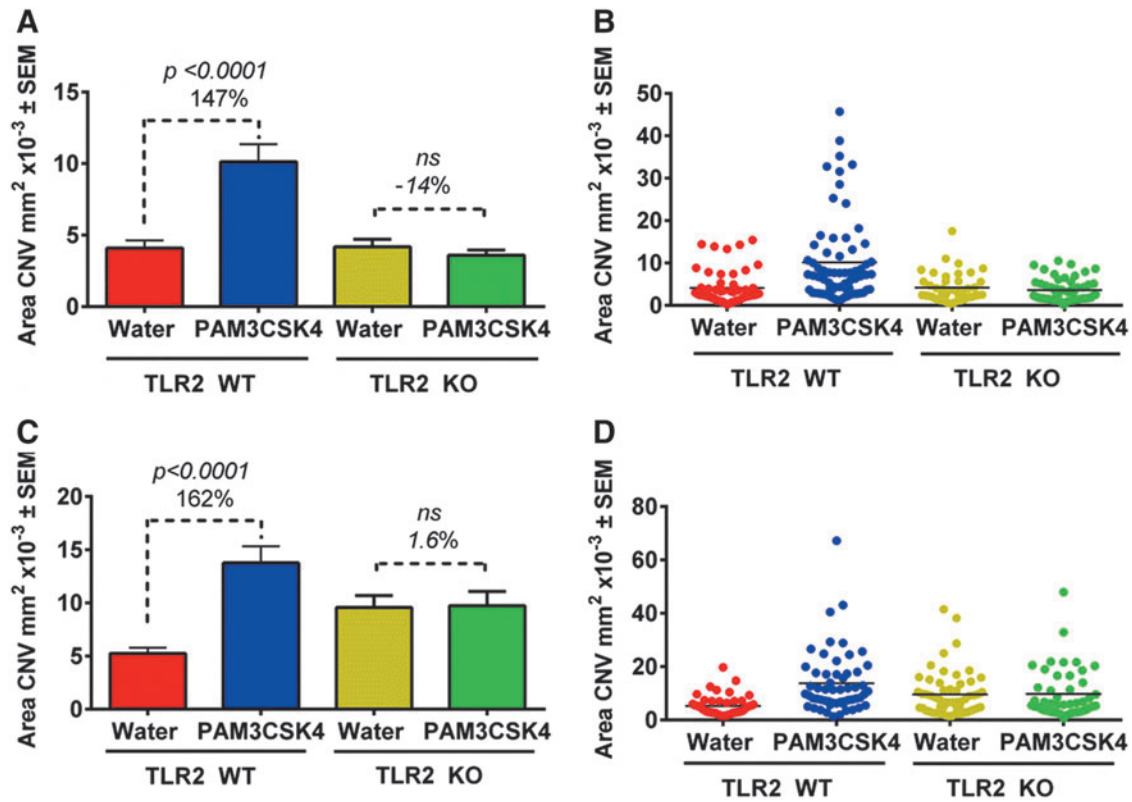


FIG. 4. TLR-2 genetic deletion abrogates the effect of PAM on CNV area growth. (A) and (C) Bar graph shows mean area of CNV ± SEM and (B) and (D) Dot plot of data from 2 independent experiments evaluating area of CNV in TLR-2 KO mice with littermate sex-matched wild-type controls. One study was with females (A) and 1 with males (C). Mice were injected i.p. with 50 µg of PAM or with water ($n=9-13$ mice, 18–26 eyes, 54–78 CNV area analyzed/condition). Statistics assessed with an unpaired t -test. $P>0.05$. WT, wild type.

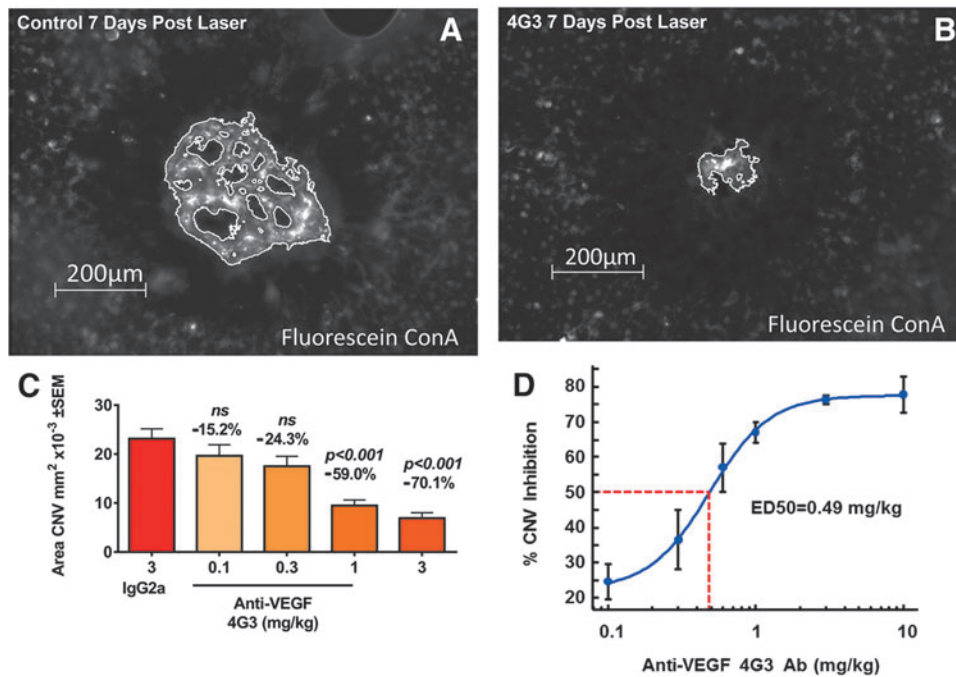


FIG. 5. Systemic administration of VEGF Ab, 4G3, dose dependently inhibits CNV lesion area labeled with Fluorescein Concanavalin A (FL-1001; Vector Laboratories). 4G3 or vehicle control was administered i.p. on day 0, 2, and 4 after laser application and CNV area measured on day 7. Representative image of CNV from mice administered (A) control or (B) 3 mg/kg 4G3. (C) Bar graph from a representative efficacy study of 4G3 in laser CNV model. Numbers above the bar are % change of CNV area relative to the mice treated with control IgG. (D) ED₅₀ (efficacy dose–response demonstrating 50% effect) curve of 4G3 generated from 27 independent efficacy studies; error bars are standard error of mean. Scale bar (A) and (B) 200 µm. Statistics assessed with a 1 way ANOVA and a Dunnett’s multiple comparison test. $P>0.05$.

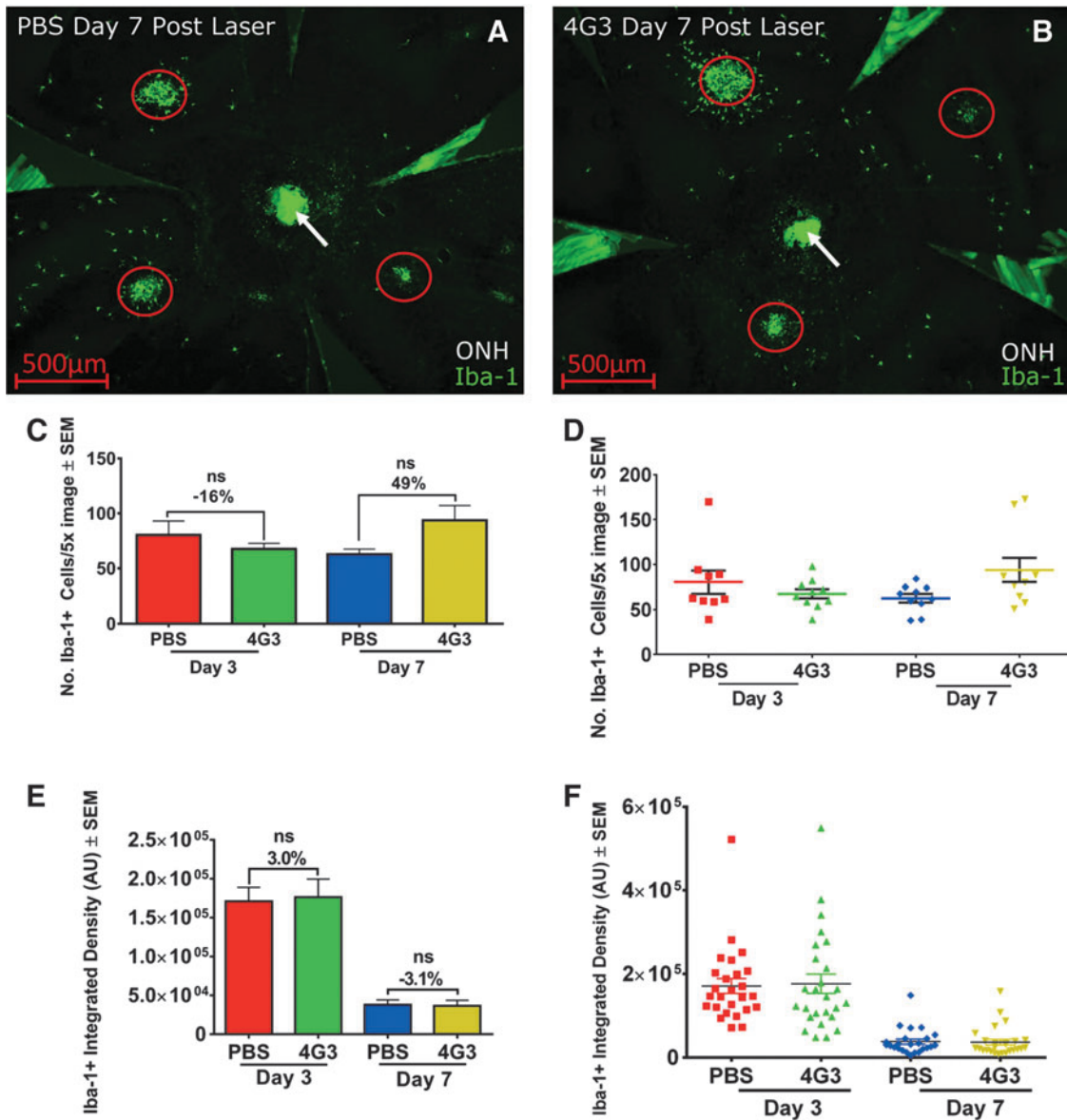


FIG. 6. Iba1⁺ cell infiltration after laser is not reduced by anti-VEGF therapy. Representative 5× images of mouse PEC collected 7 days after laser labeled with Iba1⁺ treated with (A) PBS or (B) 4G3. CNV lesions are circled. (C) Bar graph and (D) Dot plot of mean number of discrete Iba1⁺ cells peripheral to CNV lesions ($n=5$ mice, 9–10 data points per condition). (E) Bar graph and (F) Dot plot of mean integrated intensity of Iba1⁺ label in ROI centered on CNV ($n=5$ mice, 24–26 data points included in analysis/condition, $P>0.05$). Scale bar = 500 μm. ONH, optic nerve head (arrow). AU, arbitrary units; ROI, region of interest.

and photoreceptor pathology in genetic and light damage mouse models of retinal degeneration.^{50–52} We found that systemic administration of a TLR-2 activating peptide increases subretinal Iba1⁺ cellular infiltration and the area of CNV in response to laser injury. The TLR-2 activator also increased the number of infiltrating neutrophils into the CNV lesion with a large effect 24 h after administration. This neutrophil infiltration following TLR-2 activation was solely at the CNV lesion, not in the peripheral tissue, suggesting a CNV specific neutrophil chemoattractant. As neutrophils may contribute to angiogenesis,⁵³ further experiments investigating neutrophil inhibition would address the relative contribution of MNPs to the TLR-2 enhancement of CNV area.

Inhibiting TLR activity might reduce the risk of bystander cell damage from activated MNPs; however, the risk/benefit

of TLR modulation is challenging to predict. Inhibition of innate immunity associated with TLR enhances susceptibility and overall retinal destruction in response to bacterial and fungal infections.^{54,55} A reduction in the ability to respond to danger signals risks exacerbation of AMD-related RPE and photoreceptor dysfunction due to accumulation of cellular debris or other toxic material.

Others have observed that Ccl2 deletion reduces CNV in aging mice or reduces laser-induced CNV and reduced macrophage number.^{34,56} In contrast to published findings, we observed minimal changes in MNP infiltrate and increased angiogenesis in Ccl2 KO mice compared to wild-type littermate controls. Laser-induced CNV area can be quite different in the same strain of mice from different vendors, from nonlittermate controls or even the same strain of mice from 1 vendor over

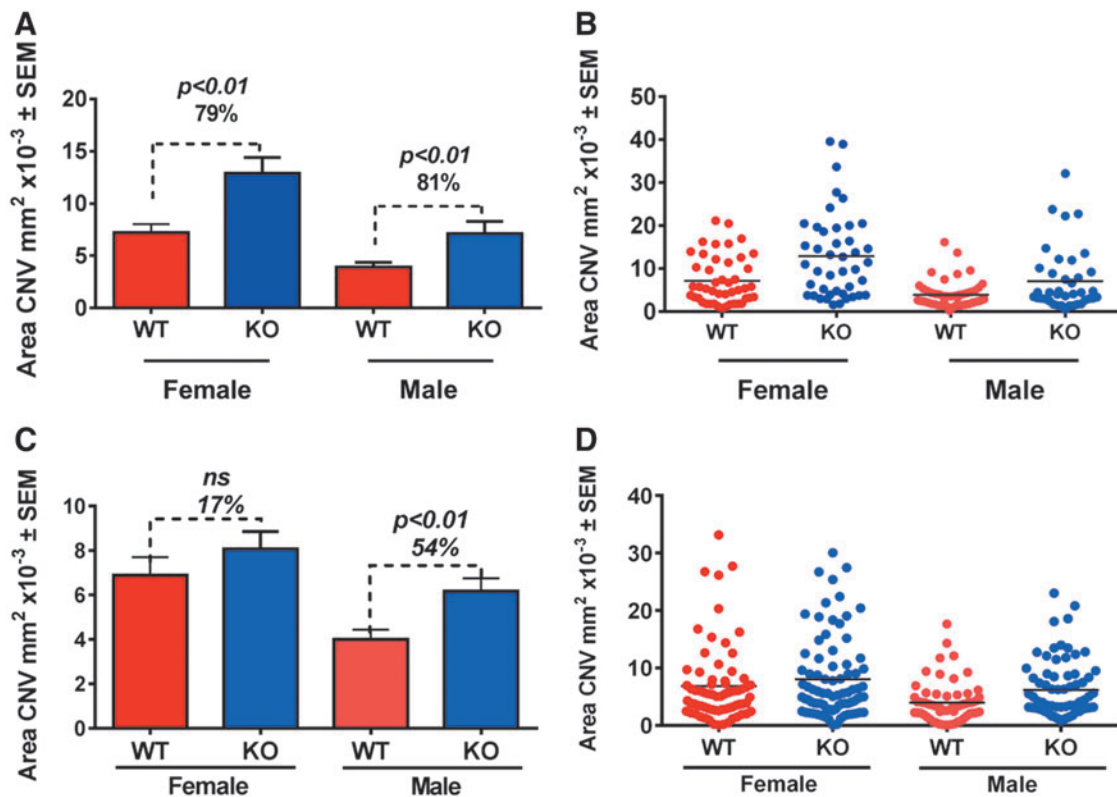


FIG. 7. Ccl2 KO mice exhibit larger CNV area compared to wild-type littermate controls. (A, C) Bar graphs and (B, D) Dot plots of mean area of CNV ± SEM of individual data points ($n=2$ studies/gender, $n=9-15$ mice/group, $n=41-81$ data points analyzed/group/study, $P \leq 0.01$ in 3 studies, $P > 0.05$ in 1 study) in 2 independent replicates. Statistics was assessed with an unpaired *t*-test.

time.³⁸ Possible explanations for the divergent observations of our experiments compared to published findings may be a different technique of measuring CNV (CNV area on flat mounts vs. area of pixels of an image of fluorescein leakage), differences in the background of the mouse strain, and finally using littermate controls versus nonlittermate controls.^{34,57} Ccl2 KO reduced MNP infiltration and was protective of retinal degeneration in CX3CR1 KO mice.³⁵ The environment in this degenerative model is likely quite different from the 1 present in laser CNV. The phenotype of the cellular infiltrates in this acute mouse laser-injury model is also likely to be different from infiltrates present in AMD. The laser model is predictive of anti-VEGF therapy for AMD, but predictability for Ccl2 remains to be determined.

Further investigation into the changes of MNP phenotype in laser CNV or spontaneous CNV would address the discrepant response we have observed in Ccl2 KO mice compared to published findings. Utilizing Polysialic⁴⁷ acid as a MNP recruitment inhibitor could shed light on the role of MNPs in neovessel formation.

TLR-2 activation significantly increases CNV angiogenesis and Iba1⁺ cell infiltration into the subretinal space and on the CNV lesion. Ccl2 genetic deletion also enhances CNV area, but in contrast, has minimal effect on numbers of infiltrating Iba1⁺ inflammatory cell. Adding to this puzzle, VEGF inhibition reduces angiogenesis but does not reduce Iba1⁺ cellular infiltrate. Reduction of macrophage infiltration reduces CNV area.^{58,59} Therefore, cellular infiltrate is not predictive of the amount of angiogenesis.

Many AMD patients still lose vision or have a degree of visual impairment; additional therapies addressing the underlying disease mechanisms beyond VEGF therapy are needed. Modulation of MNP infiltration may have unforeseen consequences. Therefore, additional assays are needed to preclinically characterize immune cells, RPE, and photoreceptor function to aid development of the next generation of AMD therapies.

Author Disclosure Statement

All authors were employees of the Novartis Institutes for Biomedical Research at the time the studies were performed.

References

- Jager, R.D., Mieler, W.F., and Miller, J.W. Age-related macular degeneration. *N. Engl. J. Med.* 358:2606–2617, 2008.
- Kauppinen, A., Paterno, J.J., Blasiak, J., Salminen, A., and Kaarniranta, K. Inflammation and its role in age-related macular degeneration. *Cell. Mol. Life. Sci.* 73:1765–1786, 2016.
- Ozaki, E., Campbell, M., Kiang, A.S., Humphries, M., Doyle, S.L., and Humphries, P. Inflammation in age-related macular degeneration. *Adv. Exp. Med. Biol.* 801:229–235, 2014.
- Chia, E.M., Wang, J.J., Roctchina, E., Smith, W., Cumming, R.R., and Mitchell, P. Impact of bilateral visual impairment on health-related quality of life: the Blue Mountains Eye Study. *Invest. Ophthalmol. Vis. Sci.* 45:71–76, 2004.

5. Cherepanoff, S., McMenamin, P., Gillies, M.C., Kettle, E., and Sarks, S.H. Bruch's membrane and choroidal macrophages in early and advanced age-related macular degeneration. *Br. J. Ophthalmol.* 94:918–925, 2010.
6. Indaram, M., Ma, W., Zhao, L., Fariss, R.N., Rodriguez, I.R., and Wong, W.T. 7-Ketocholesterol increases retinal microglial migration, activation, and angiogenicity: a potential pathogenic mechanism underlying age-related macular degeneration. *Sci. Rep.* 5:9144, 2015.
7. Rodriguez, I.R., Clark, M.E., Lee, J.W., and Curcio, C.A. 7-ketocholesterol accumulates in ocular tissues as a consequence of aging and is present in high levels in drusen. *Exp. Eye. Res.* 128:151–155, 2014.
8. Ma, W., and Wong, W.T. Aging changes in retinal microglia and their relevance to age-related retinal disease. *Adv. Exp. Med. Biol.* 854:73–78, 2016.
9. Kandasamy, R., Wickremasinghe, S., and Guymer, R. New treatment modalities for geographic atrophy. *Asia Pac. J. Ophthalmol. (Phila.)* 6:508–513, 2017.
10. Prasad, P.S., Schwartz, S.D., and Hubschman, J.P. Age-related macular degeneration: current and novel therapies. *Maturitas.* 66:46–50, 2010.
11. Karlstetter, M., Scholz, R., Rutar, M., Wong, W.T., Provis, J.M., and Langmann, T. Retinal microglia: just bystander or target for therapy? *Prog. Retin. Eye. Res.* 45:30–57, 2015.
12. Walker, F.R., Nilsson, M., and Jones, K. Acute and chronic stress-induced disturbances of microglial plasticity, phenotype and function. *Curr. Drug. Targets.* 14:1262–1276, 2013.
13. Lull, M.E., and Block, M.L. Microglial activation and chronic neurodegeneration. *Neurotherapeutics.* 7:354–365, 2010.
14. Scholz, R., Caramoy, A., Bhuckory, M.B., et al. Targeting translocator protein (18 kDa) (TSPO) dampens pro-inflammatory microglia reactivity in the retina and protects from degeneration. *J. Neuroinflammation.* 12:201, 2015.
15. Buschini, E., Piras, A., Nuzzi, R., and Vercelli, A. Age related macular degeneration and drusen: neuroinflammation in the retina. *Prog. Neurobiol.* 95:14–25, 2011.
16. Gupta, N., Brown, K.E., and Milam, A.H. Activated microglia in human retinitis pigmentosa, late-onset retinal degeneration, and age-related macular degeneration. *Exp. Eye. Res.* 76:463–471, 2003.
17. Xu, H., Chen, M., and Forrester, J.V. Para-inflammation in the aging retina. *Prog. Retin. Eye. Res.* 28:348–368, 2009.
18. Levy, O., Calippe, B., Lavalette, S., et al. Apolipoprotein E promotes subretinal mononuclear phagocyte survival and chronic inflammation in age-related macular degeneration. *EMBO. Mol. Med.* 7:211–226, 2015.
19. Singh, P.K., and Kumar, A. Retinal photoreceptor expresses toll-like receptors (TLRs) and elicits innate responses following TLR ligand and bacterial challenge. *PLoS. One.* 10:e0119541, 2015.
20. Stewart, E.A., Wei, R., Branch, M.J., Sidney, L.E., and Amoaku, W.M. Expression of Toll-like receptors in human retinal and choroidal vascular endothelial cells. *Exp. Eye. Res.* 138:114–123, 2015.
21. Kim, Y.W., Yakubenko, V.P., West, X.Z., et al. Receptor-mediated mechanism controlling tissue levels of bioactive lipid oxidation products. *Circ. Res.* 117:321–332, 2015.
22. Salomon, R.G., Hong, L., and Hollyfield, J.G. Discovery of carboxyethylpyrroles (CEPs): critical insights into AMD, autism, cancer, and wound healing from basic research on the chemistry of oxidized phospholipids. *Chem. Res. Toxicol.* 24:1803–1816, 2011.
23. Seimon, T.A., Nadolski, M.J., Liao, X., et al. Atherogenic lipids and lipoproteins trigger CD36-TLR2-dependent apoptosis in macrophages undergoing endoplasmic reticulum stress. *Cell. Metab.* 12:467–482, 2010.
24. Shaw, P.X., Stiles, T., Douglas, C., et al. Oxidative stress, innate immunity, and age-related macular degeneration. *AIMS. Mol. Sci.* 3:196–221, 2016.
25. Fujimoto, T., Sonoda, K.H., Hijioka, K., et al. Choroidal neovascularization enhanced by Chlamydia pneumoniae via Toll-like receptor 2 in the retinal pigment epithelium. *Invest. Ophthalmol. Vis. Sci.* 51:4694–4702, 2010.
26. Luckoff, A., Caramoy, A., Scholz, R., Prinz, M., Kalinke, U., and Langmann, T. Interferon-beta signaling in retinal mononuclear phagocytes attenuates pathological neovascularization. *EMBO. Mol. Med.* 8:670–678, 2016.
27. Pikuleva, I.A., and Curcio, C.A. Cholesterol in the retina: the best is yet to come. *Prog. Retin. Eye. Res.* 41:64–89, 2014.
28. Sarks, J.P., Sarks, S.H., and Killingsworth, M.C. Morphology of early choroidal neovascularisation in age-related macular degeneration: correlation with activity. *Eye. (Lond).* 11:515–522, 1997.
29. Kabba, J.A., Xu, Y., Christian, H., et al. Microglia: housekeeper of the Central Nervous System. *Cell. Mol. Neurobiol.* 38:53–71, 2018.
30. Dewald, O., Zymek, P., Winkelmann, K., et al. CCL2/Monocyte Chemoattractant Protein-1 regulates inflammatory responses critical to healing myocardial infarcts. *Circ. Res.* 96:881–889, 2005.
31. Semple, B.D., Bye, N., Rancan, M., Ziebell, J.M., and Morganti-Kossmann, M.C. Role of CCL2 (MCP-1) in traumatic brain injury (TBI): evidence from severe TBI patients and CCL2-/- mice. *J. Cereb. Blood. Flow. Metab.* 30:769–782, 2010.
32. Takahashi, M., Galligan, C., Tessarollo, L., and Yoshimura, T. Monocyte chemoattractant protein-1 (MCP-1), not MCP-3, is the primary chemokine required for monocyte recruitment in mouse peritonitis induced with thioglycollate or zymosan A. *J. Immunol.* 183:3463–3471, 2009.
33. Hagbi-Levi, S., Grunin, M., Elbaz-Hayoun, S., et al. Retinal phenotype following combined deletion of the chemokine receptor CCR2 and the chemokine CX3CL1 in mice. *Ophthalmic. Res.* 55:126–134, 2016.
34. Robbie, S.J., Georgiadis, A., Barker, S.E., et al. Enhanced Ccl2-Ccr2 signaling drives more severe choroidal neovascularization with aging. *Neurobiol. Aging.* 40:110–119, 2016.
35. Sennlaub, F., Auvynet, C., Calippe, B., et al. CCR2(+) monocytes infiltrate atrophic lesions in age-related macular disease and mediate photoreceptor degeneration in experimental subretinal inflammation in Cx3cr1 deficient mice. *EMBO. Mol. Med.* 5:1775–1793, 2013.
36. Ambati, J., Anand, A., Fernandez, S., et al. An animal model of age-related macular degeneration in senescent Ccl-2- or Ccr-2-deficient mice. *Nat. Med.* 9:1390–1397, 2003.
37. Jonas, J.B., Tao, Y., Neumaier, M., and Findeisen, P. Monocyte chemoattractant protein 1, intercellular adhesion molecule 1, and vascular cell adhesion molecule 1 in exudative age-related macular degeneration. *Arch. Ophthalmol.* 128:1281–1286, 2010.
38. Poor, S.H., Qiu, Y., Fassbender, E.S., et al. Reliability of the mouse model of choroidal neovascularization induced by laser photocoagulation. *Invest. Ophthalmol. Vis. Sci.* 55:6525–6534, 2014.

39. Combadiere, C., Feumi, C., Raoul, W., et al. CX3CR1-dependent subretinal microglia cell accumulation is associated with cardinal features of age-related macular degeneration. *J. Clin. Invest.* 117:2920–2928, 2007.
40. Huang, H., Parlier, R., Shen, J.K., Luty, G.A., and Viores, S.A. VEGF receptor blockade markedly reduces retinal microglia/macrophage infiltration into laser-induced CNV. *PLoS. One.* 8:e71808, 2013.
41. Kawai, T., and Akira, S. The role of pattern-recognition receptors in innate immunity: update on Toll-like receptors. *Nat. Immunol.* 11:373–384, 2010.
42. Krause, T.A., Alex, A.F., Engel, D.R., Kurts, C., and Eter, N. VEGF-production by CCR2-dependent macrophages contributes to laser-induced choroidal neovascularization. *PLoS. One.* 9:e94313, 2014.
43. Rymo, S.F., Gerhardt, H., Wolfhagen Sand, F., Lang, R., Uv, A., and Betsholtz, C. A two-way communication between microglial cells and angiogenic sprouts regulates angiogenesis in aortic ring cultures. *PLoS. One.* 6:e15846, 2011.
44. Gao, F., Hou, H., Liang, H., Weinreb, R.N., Wang, H., and Wang, Y. Bone marrow-derived cells in ocular neovascularization: contribution and mechanisms. *Angiogenesis.* 19:107–118, 2016.
45. Rutar, M., and Provis, J.M. Role of chemokines in shaping macrophage activity in AMD. *Adv. Exp. Med. Biol.* 854:11–16, 2016.
46. Luckoff, A., Scholz, R., Sennlaub, F., Xu, H., and Langmann, T. Comprehensive analysis of mouse retinal mononuclear phagocytes. *Nat. Protoc.* 12:1136–1150, 2017.
47. Karlstetter, M., Kopatz, J., Aslanidis, A., et al. Polysialic acid blocks mononuclear phagocyte reactivity, inhibits complement activation, and protects from vascular damage in the retina. *EMBO. Mol. Med.* 9:154–166, 2017.
48. Li, L., Eter, N., and Heiduschka, P. The microglia in healthy and diseased retina. *Exp. Eye. Res.* 136:116–130, 2015.
49. West, X.Z., Malinin, N.L., Merkulova, A.A., et al. Oxidative stress induces angiogenesis by activating TLR2 with novel endogenous ligands. *Nature.* 467:972–976, 2010.
50. Ko, M.K., Saraswathy, S., Parikh, J.G., and Rao, N.A. The role of TLR4 activation in photoreceptor mitochondrial oxidative stress. *Invest. Ophthalmol. Vis. Sci.* 52:5824–5835, 2011.
51. Kohno, H., Chen, Y., Kevany, B.M., et al. Photoreceptor proteins initiate microglial activation via Toll-like receptor 4 in retinal degeneration mediated by all-trans-retinal. *J. Biol. Chem.* 288:15326–15341, 2013.
52. Syeda, S., Patel, A.K., Lee, T., and Hackam, A.S. Reduced photoreceptor death and improved retinal function during retinal degeneration in mice lacking innate immunity adaptor protein MyD88. *Exp. Neurol.* 267:1–12, 2015.
53. Liang, W., and Ferrara, N. The complex role of neutrophils in tumor angiogenesis and metastasis. *Cancer. Immunol. Res.* 4:83–91, 2016.
54. Novosad, B.D., Astley, R.A., and Callegan, M.C. Role of Toll-like receptor (TLR) 2 in experimental *Bacillus cereus* endophthalmitis. *PLoS. One.* 6:e28619, 2011.
55. Talreja, D., Singh, P.K., and Kumar, A. In vivo role of TLR2 and MyD88 signaling in eliciting innate immune responses in staphylococcal endophthalmitis. *Invest. Ophthalmol. Vis. Sci.* 56:1719–1732, 2015.
56. Tsutsumi, C., Sonoda, K.H., Egashira, K., et al. The critical role of ocular-infiltrating macrophages in the development of choroidal neovascularization. *J. Leukoc. Biol.* 74:25–32, 2003.
57. Luhmann, U.F., Robbie, S., Munro, P.M., et al. The drusenlike phenotype in aging *Ccl2*-knockout mice is caused by an accelerated accumulation of swollen autofluorescent subretinal macrophages. *Invest. Ophthalmol. Vis. Sci.* 50:5934–5943, 2009.
58. Jawad, S., Liu, B., Li, Z., et al. The role of macrophage class a scavenger receptors in a laser-induced murine choroidal neovascularization model. *Invest. Ophthalmol. Vis. Sci.* 54:5959–5970, 2013.
59. Espinosa-Heidmann, D.G., Suner, I.J., Hernandez, E.P., Monroy, D., Csaky, K.G., and Cousins, S.W. Macrophage depletion diminishes lesion size and severity in experimental choroidal neovascularization. *Invest. Ophthalmol. Vis. Sci.* 44:3586–3592, 2003.

Received: November 22, 2017

Accepted: May 14, 2018

Address correspondence to:

Dr. Stephen H. Poor
Department of Ophthalmology
Novartis Institutes for Biomedical Research
22 Windsor Street
Cambridge, MA 02139

E-mail: stephen.poor@novartis.com